Energy Conversion and Management: X 24 (2024) 100768

Contents lists available at ScienceDirect

Energy Conversion and Management: X

journal homepage: www.sciencedirect.com/journal/energy-conversion-and-management-x

Predictive control technique for solar photovoltaic power forecasting

Nsilulu T. Mbungu [a,b], Safia Babikir Bashir [a], Neethu Elizabeth Michael [a], Mena Maurice Farag [a], Abdul-Kadir Hamid [a,c], Ali A. Adam Ismail [a,c,d], Ramesh C. Bansal [a,c,f], Ahmed G. Abo-Khalil [a,e], A. Elnady [a,c], Mousa Hussein [g,*]

[a] Research Institute of Sciences and Engineering (RISE), University of Sharjah, Sharjah, United Arab Emirates
[b] Department of Electrical Engineering, Tshwane University of Technology, Pretoria, South Africa
[c] Department of Electrical Engineering, University of Sharjah, Sharjah, United Arab Emirates
[d] Department of Electrical Engineering, Omdurman Islamic University, Omdurman, Sudan
[e] Department of Sustainable and Renewable Energy Engineering, University of Sharjah, Sharjah, United Arab Emirates
[f] Department of Electrical, Electronic and Computer Engineering, University of Pretoria, Pretoria, South Africa
[g] Department of Electrical and Communication Engineering, United Arab Emirates University, Al Ain, United Arab Emirates

ARTICLE INFO

Keywords:
Energy estimation
Power forecast
Renewable energy resource
Machine learning
Model predictive control
Photovoltaic
Solar power

ABSTRACT

An accurate estimation of photovoltaic (PV) power production is crucial for organizing and regulating solar PV power plants. The suitable prediction is often affected by the variable nature of solar resources, system location and some internal/external disturbances, such as system effectiveness, climatic factors, etc. This paper develops a novel strategy for applying a predictive control technique to PV power forecasting applications in a smart grid environment. The strategy develops the model predictive control (MPC) under demand response (DR) and some data-driven methods. It has been found that it is challenging to model an MPC for solar power forecasting regardless of its robustness and ability to handle constraints and disturbance. Thus, an optimal quadratic performance index-based MPC scheme is formulated to model a forecasting method for a PV power prediction. This strategy is then compared with some machine learning approaches. The developed strategies solve the problem of accurately estimating the direct current (DC) power yielded from the PV plant in a real-world implementation. The study also considers external disturbances to evaluate the significance of the developed methods for a suitable forecast. Therefore, this study optimally demonstrates that an accurate solar PV DC power prediction can relatively be estimated with an appropriate strategy, such as MPC and MLs, considering the system disturbances. This study also offers promising results for intelligent and real-time energy resource estimation that assist in developing the solar power sector.

1. Introduction

Solar power is a game-changing resource of modern energy systems to support sustainable development goals. For instance, all renewable energy resources, from geothermal passing hydro systems to wind power, depend on solar power [1]. The diversity of energy sources in this modern world is a key figure in maintaining the resilience and reliability of the electrical grid. Distributed energy resources based on variable renewable energies are increasingly being implemented in several countries worldwide [2,3]. Therefore, solar power is considered one of the best sustainable energy resources to enhance the performance of the utility grid, which is challenged by intensive demand growth [1]. The estimated power-generating resource for a reliable electrical network is suitable for ensuring its effectiveness. Besides, the uncertainty of variable renewable energy necessitates a robust control method to provide a secure power supply [4,5]. The application of forecast modelling effectively assists in the estimation of variable renewable energy. This can be modelled using modelling and/or data-driven strategies [6].

Solar power plants are increasing and getting more attention in the primary electricity grid, resulting from the high penetration of independent power producers derived from renewable energy sources. Thus, the smart grid technologies offer opportunities to plan, control, monitor, supervise and distribute the independent power producers [7,8]. The power system consistently requires the prediction results of different input sources to meet the energy demand and plan the future [9]. Manual computations, empirical formulae, and simplified predictions based on historical data and climatic characteristics are all used in conventional approaches to forecast solar energy [10,11].

* Corresponding author.
E-mail address: mihussein@uaeu.ac.ae (M. Hussein).

https://doi.org/10.1016/j.ecmx.2024.100768
Received 17 July 2024; Received in revised form 20 September 2024; Accepted 19 October 2024
Available online 29 October 2024

Nomenclature

A_{pv}	PV panel surface [m^2]
N	Time horizon of the system design
t	Sampling time [minute]
η_{inv}	Inverter efficiency of the BESS
η_{pv}	PV panel efficiency
I_{pv}	Solar irradiation incident measured on the PV panel [kW/m^2]
J	Objection function
P_{ba}	Power flow on the BESS
P_{pv}	Generated power by the PV
Δt	Time variation [minute]
AC	Alternative Current
DC	Direct Current
DER	Distributed Energy Resource
DG	Distributed Generation
DSM	Demand Side Management
MPC	Model Predictive Control
MPPT	Maximum Power Point Tracker
PV	Photovoltaic
RER	Renewable Energy Resource
RMS	Root Means Square
RTP	Real-Time Pricing

These methods can be laborious and vulnerable to errors since they frequently need substantial human work and skill to examine and interpret the data, resulting in less precise forecasts [12,13]. Therefore, it is essential to conduct prediction studies and accurately yield estimates of solar power generation. In addition, several published works have developed strategies for solar power forecasting using data-driven and model-based methods under predictive control techniques.

Machine learning (ML) algorithms transform solar energy forecasts using cutting-edge computational methodologies. ML methods can capture dynamic interactions between factors and adapt to changing circumstances, producing more accurate and trustworthy predictions for solar energy [14]. A variety of practical solar forecasting techniques are available, including statistical, persistence, physical, and sophisticated hybrid models [15]. Statistical models are again classified into time series models and artificial neural networks (ANN) models, whereas physical models consist of numerical weather prediction models. Sophisticated hybrid models include genetic algorithm, fuzzy logic, ANN combined fuzzy, ANN combined genetic algorithm, maximum likelihood estimation, and more [16,17]. In [18], a day-ahead strategy for the solar power forecasting model is presented. The system design is modelled using the numerical weather prediction model to optimally forecast the energy from the photovoltaic (PV) power plants. A suitable positive correlation between the observed and forecasted output power has been observed. Deep learning (DL) strategies can also be used to investigate the efficacy, productivity, and possible uses of solar energy potential [14]. In contrast, ML models like ANN are effectively being used to forecast solar energy output [19].

Recurrent neural networks (RNN) and convolutional neural networks (CNN) performed better than some AI-based practices; however, the feature is retrieved in spatial dimensions with CNN, and solar power generation incorporates both spatial and temporal characteristics [20]. However, the majority of studies are more focused on the prediction capabilities of CNN-RNN, leading to a mixture of solutions. A methodical description of the CNN-RNN system for multivariate data is currently inadequate. Moreover, it is not evident which architectures could produce the best forecasting results [21]. In Xingtai City, northern China, Meng et al. [22] employed datasets with bright, overcast, and wet days to conduct random forest (RF) forecast studies. The ultimate outcomes were calculated by averaging the regression findings for each data set. The RF method outperforms better than other ML models because it can take advantage of past feature values, and it provides an accurate prediction.

Aprillia, H et al. [23] introduced an innovative approach that combines the CNN with the salp swarm procedure for predicting power from a solar PV system. Through a salp swarm algorithm, developers can optimize the best parameters for each CNN regression. The suggested strategies are tested for effectiveness by comparing them to the salp swarm algorithm vector support and the long-term neural memory network-based salp swarm algorithm. Ref. [24] observed that the convolutional self-attention-based long short-term memory (LSTM) architecture increases the precision of predictions by gathering specific information from the context and producing locally applicable variables and concerns. Solar power production estimates use actual data and power demand forecasts to evaluate system implementation, lowering energy consumption when compared with canonical deep neural networks, LSTM, and self-attention-based LSTM models. Abdulai et al. [25] cover data analytics strategies for solar power prediction, such as statistical models, ML, and ANN.

Ahn et al. [26] suggested a deep RNN under a short-term forecasting method to predict 12-time steps and 3 RNN layers for solar power generation. They attained excellent accuracy in their short-term prediction study. Similarly, Harrou et al. [27] suggested a multidimensional LSTM approach in their research on PV power prediction under multiple environmental factors, including ambient temperature, wind speed, cell temperature and more, that are added to the solar irradiation variables to improve model accuracy. Gao et al. [28] examined three prediction situations, including cloudy, overcast and rainy. They extrapolated that the LSTM method is the most appropriate and adequate at portraying the shifting character of solar energy production.

The model predictive control (MPC) algorithm is a groundbreaking method that has dramatically acquired recognition in several optimal control operations [29]. Due to its adaptability in how functions are executed and the speed of its processors, the MPC approach has received widespread attention [30]. For instance, through the MPC framework, a hybrid prediction model with both long and short terms was verified within a measured dataset from an actual Japanese office building energy system. The findings demonstrate that the suggested hybrid prediction MPC framework enhanced the results by 81.6% when compared to the baseline control logic [31]. Ref. [32] develop a mixed strategy for PV power prediction under artificial neural networks (ANN) and seasonal auto-regressive integrated moving average in the design framework conceptual of MPC applications. This strategy is formulated using a short-term forecast method with a prediction horizon of 15 min. The developed hybrid approach increases the redundancy and resilience of the forecast approach and minimizes the forecast error compared to a no-hybrid strategy. In [33], a stochastic MPC is applied to control the thermal solar collector fields. This strategy also considers predicting the solar irradiance forecast within an uncertain environment. It has been demonstrated in [6] that predictive control techniques can be designed under several strategies, including the MPC algorithm, ML and more, to estimate and/or predict diverse variables of energy resources. It is also observed that the MPC strategy has not yet been developed for solar power forecasting applications. Therefore, this study seeks to address this chasm by developing a novel strategy for model-based MPC to accurately forecast solar PV power generation.

Table 1 presents a comprehensive assessment of some relevant published works narrowed down into the developed approaches of this study in order to observe their contributions, detail gaps and provide the novelty of this study. Therefore, this work looks at the system performance for practical estimation of solar power forecasts by applying a predictive control technique. MPC and various ML strategies have been developed to formulate the system dynamic that can forecast the electrical energy generated by a solar PV system. ML strategies

Table 1
A comprehensive overview assessment of various studied approaches in solar PV power forecasting.

Papers	MPC & ML approaches					Observation of contributions	
Ref.: Year	MPC	CNN	RF	CNN-RF	BiLSTM-GRU	DR	PV power forecasting
[35]: 2024	✗	✓	✗	✗	✗	✗	✓: day-ahead regional power
[36]: 2024	✗	✓	✗	✗	✓	✗	✗: solar irradiance forecasting
[33]: 2024	✓	✗	✗	✗	✗	✗	✗: solar thermal plant control
[37]: 2023	✗	✗	✓	✗	✗	✗	✓: short-term prediction
[38]: 2022	✗	✓	✗	✗	✓	✗	✓: weekly power forecasting
[39]: 2021	✗	✗	✓	✓	✗	✗	✗: solar irradiance forecasting
[40]: 2021	✗	✓	✗	✗	✗	✗	✓: monthly power prediction
[41]: 2020	✗	✓	✗	✗	✗	✗	✓: day-ahead in grid-tied PV
[22]: 2020	✗	✗	✓	✗	✗	✗	✓: daily power forecasting
[35]: 2019	✗	✗	✓	✗	✗	✗	✓: great accuracy/robustnees
This work	✓	✓	✓	✓	✓	✓	✓: MPC under DR scheme and some MLs for a week power forecasting, considering disturbance, are developed for a grid-tied PV application.

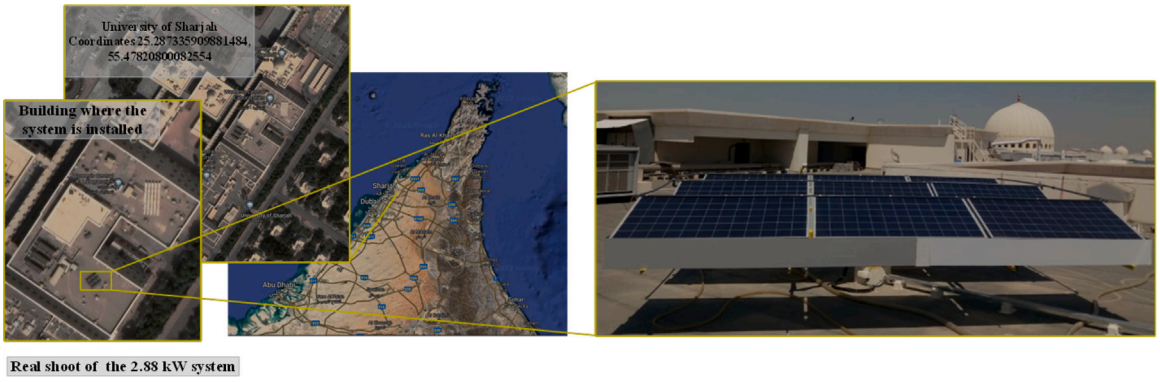

Fig. 1. Established 2.88 kW on-grid PV/T system in University of Sharjah, UAE.

are CNN, RF, CNN-RF, and DL-based bidirectional LSTM (BiLSTM) and gated-recurrent unit (GRU). Therefore, the developed strategies look to model the predictive behaviour of solar direct current (DC) electricity supply output through the conceptual framework of dynamic forecasts. The advantage of the developed strategies using predictive and intelligent schemes is also demonstrated by their capability to handle various disturbances [6]. The application of intelligent schemes offers several opportunities for dynamic modelling in several research, development and innovation fields [34]. Therefore, this study also examines the performance of each model during the disturbance that affects solar radiation to assess the performance metrics of the designed strategies. The leading contributions of this work are emphasized as outlined:

- Develop optimal solar PV forecasting strategies by applying system modelling and data-driven methods to predict the power forecast from a real-world implementation of a solar PV system.
- Design a mode-based DC power forecast in the framework system analysis that combines the generating energy from the PV system with the demand response scheme. This strategy formulates the state-space model based on generating energy from solar PV to develop a DC power forecast under the MPC strategy. This approach also demonstrates the impact of the developed MPC in a moving horizon window that handles constraints and disturbance and deals with control horizon and weighted parameters for an optimal DC power prediction.
- Implement data-driven methods that use the data from the solar PV power plant within a given month to predict the dynamic behaviour of future DC power for the last seven days of the selected month. Therefore, this model-free technique is developed using ML approaches, including RF, CNN, hybrid CNN-F and hybrid BiSLTM-GRU.
- A comparative analysis of MPC and ML methods is also performed to assess the performance of the developed approaches. This assessment considers the performance metrics of each proposed strategy to analyse its effectiveness and evaluate its prediction impact in terms of optimal DC power forecasts from solar PV systems.

The remaining sections of this work are presented as follows: The experimental system and its implementation, including data analysis and desired performance metrics, are detailed in Section 2. Section 3 discusses system design and modelling for the developed solar PV power forecasting strategies. Section 4 presents and discusses forecasting results. The study is concluded in Section 5.

2. System configuration

Table 2 summarizes the implementation configuration for the developed forecasted methods. This is a roof-inclined 2.88 kW rated grid-integrated PV system established at the W-12 building (Lat 25.34° N; Long 55.42° E) at the main campus of the University of Sharjah, Sharjah, UAE, as presented in Fig. 1. The DC solar power for a given time horizon N is formulated in Eq. (2).

$$P_{pv}(t) = \zeta_{pv} S_{pv} \sum_{t=1}^{N} I_{pv}(t) \tag{1}$$

with ζ_{pv} is the efficiency of the PV panels, t is the sampling time of the computational horizon N, S_{pv} is the surface area of the PV [m^2], and I_{pv} represents the solar irradiance incident on the PV panels [kW/m^2]. The PV conversation efficiency can be presented in the function of the temperature as follows [13]:

$$\zeta_{pv} = \zeta_{ref}[1 + \beta(T_{pv} - T_{ref})] \tag{2}$$

Table 2
Technical specifications of established on-grid PV system.

Components	Role & Features
Solar PV Energy System	– DC unit comprises nine PV modules, each rated at 320 W. – The alternating current (AC) unit comprises a 3.7 kVA Inverter responsible for synchronization with utility grid requirements. – AC unit is also coupled with an energy metering device for constant recording of energy generated in kilowatt hour.
Data Collection Unit	– Monitor all electrical and environmental metrics through the centralization of measurement sensors. – Centralization of sensor data from common sensor box. – Use wired/wireless data logging capability for real-time data collection. – Features a cloud-supported user-friendly interface for user depiction of system overall performance.
Installed data measurement sensors	– Electrical Sensors: • Use for the measurement of DC and AC variables. – Solar Irradiance sensor: • Use for the measurement of solar irradiance in W/m^2. • Compose of monocrystalline silicon solar PV cell • ±5% of the uncertainty in the measurement – Anemometer: • Measure the wind speed of the system in m/s. • ±5% of the uncertainty in the measurement is applied to facilitate a precision of 1 m/s. – Temperature sensors: • Use for the measurement of module and ambient temperature based on PT-1000 technology. • ±0.8 °C of the uncertainty in the measurement. • Range between -50 °C to +230 °C.

with ζ_{ref} is the PV conversion efficiency at standard testing conditions, β is the temperature power coefficient, T_{pv} is the module temperature, and T_{ref} is the temperature at standard testing conditions.

2.1. Real-world implementation configuration

The installed grid-connected PV system comprises two simultaneous loops that structure the topology of the given system, which are the power and communication loops. The power loop controls the power conversion unit, i.e., the DC–AC power converter and grid synchronization requirements. The synchronization with local grid requirements is vital in achieving power quality, preventing mismatches in voltage and frequency requirements, and avoiding unexpected disconnections from the utility grid [1].

The data acquisition is centralized under a single data manager to effectively assess the system efficiency based on multiple installed electrical and environmental sensors for measurement with a 5-minute resolution per reading stored. The integrated Fronius data manager allows for flexible communication between the grid-connected inverter and the installed measurement sensors. A communication network containing a wired/wireless local area is established for seamless data transmission between the data manager and a dedicated cloud-based interface. This is successfully achieved through the dedicated IP address associated with the system that provides remote access to its performance and insights into the system's performance through analytical visual representations. Moreover, optimum and real-time monitoring is conducted based on the seamless configuration of the data manager's integrated web server, allowing the inspection system's anomalies in real time. Additionally, the real-time measurements from outdoor sensors are seamlessly integrated within the real-time monitoring package based on a Fronius sensor box, which allows for the simultaneous integration of six sensors for monitoring critical environmental parameters such as irradiance and temperature. In this notion, the data acquisition unit not only allows instantaneous monitoring of the system's performance but also exports this data for further processing and incorporates different modelling and forecasting methods associated with this study. Fig. 2 presents the system configuration of a real-world implementation, as shown in Fig. 1.

2.2. Data analysis

The forecasting methods developed in this investigation utilized a data set comprising environmental parameters, including ambient temperature, solar irradiance, module operating temperature and the speed of wind, along with the maximum DC power generated during May 2022. The data is experimentally driven from the aforementioned on-grid PV system, which observed the highest energy yield compared to other months across the year. The target objective of this work is to estimate the maximum DC power generation with the current data set to establish an accurate and precise prediction model for implementation in large-scale PV grid-connected systems under harsh weather conditions, such as Sharjah, UAE.

The heatmap in Fig. 3 reveals the interdependencies of various environmental factors regarding DC power output. This heatmap is a function of the system implementation, as presented in Fig. 1. The provided heatmap clearly emphasized how closely the performance of PV systems is related to weather conditions that keep changing. The heatmap suggests a decisive relationship between DC power and solar irradiance, as well as between DC power and module temperature. Thus emphasizing the importance of these features in the precise prediction of DC power and the final overall energy yields of the system. In another observation, the ambient temperature points towards a moderate degree of correlation, and wind speed depicts a relatively weaker correlation to the DC power.

Table 3 presents a statistical characterization of the data set. This serves to quantify the performance of the PV system and monitor environmental and election impacts. Besides, the dataset is diverse, reflecting the multifaceted nature of the system performance under varying environmental and operational conditions.

3. System modelling of forecasting methods

3.1. Model predictive control

MPC is one the robust algorithms of the predictive control techniques [6]. $\forall t \in N$, as shown in Eq. (2), $\Rightarrow t = k$, therefore, Fig. 4 demonstrates the implementation scheme of MPC for given control horizon N_c and predicted time horizon N_p with a computational time

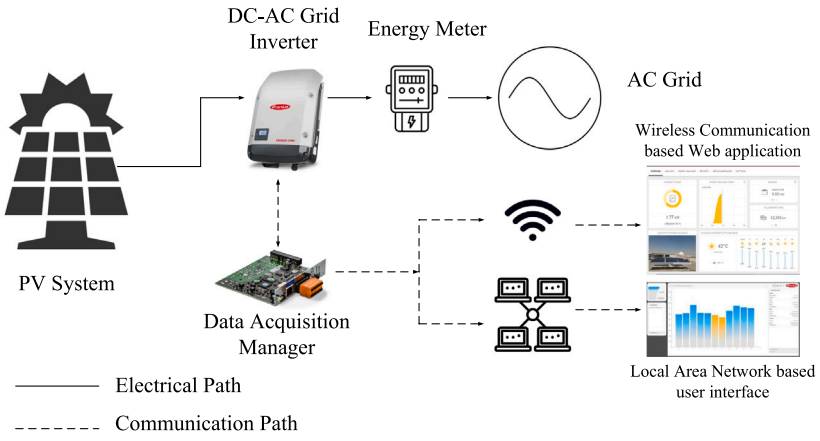

Fig. 2. Power and communication topology for the installed grid-tied PV system.

Table 3
Descriptive statistics of environmental and electrical variables.

Statistics	Ambient temperature	Wind speed	Solar irradiance	Module temperature	DC power (W)
Count	8928.00	8928.00	8928.00	8928.00	8928.00
Mean	33.12	3.15	315.55	41.39	739.55
Std	5.46	3.06	349.89	13.75	837.28
Min	23.00	0.00	0.00	23.00	0.00
25%	29.00	0.00	0.00	30.00	0.00
50%	32.00	3.00	86.00	34.99	137.84
75%	37.00	5.00	716.90	55.00	1704.56
Max	47.00	18.00	919.00	73.00	2259.52

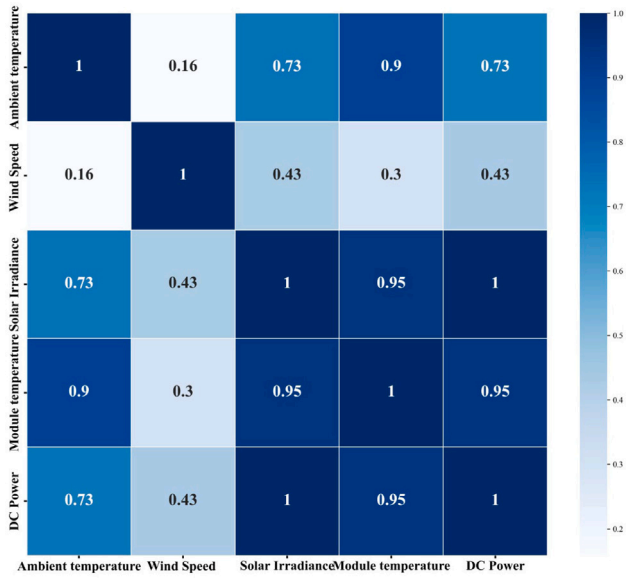

Fig. 3. Heatmap: Data assessment of the system implementation.

at a given sample k. This is a closed-loop optimal control strategy considering a receding horizon that can be applied to several industrial applications, including the forecast for distributed energy resources. Several modelling approaches can be used to implement the moving horizon window of the MPC scheme. The state-space formulation is one of the modelling approaches that is also applied in the MPC method. Therefore, Eq. (3) represents a canonical state-space model with input disturbance formulated in this study [43].

$$\begin{cases} x(k+1) &= Ax(k) + Bu(k) - B_v v(k) \\ y(k) &= Cx(k) \end{cases} \tag{3}$$

with A, B, B_v, C, and x are the state matrix, the input matrix, the scaling and mixing matrix for the process noise input, the output matrix, and the state vector; the signal being received is represented by u, v is the disturbance applied to the system, y represents the final output signal, and k is the sampling time.

By considering the real-world implementation configuration detailed in Fig. 2, the MPC solar PV power forecast strategy-based demand response under a real-time pricing scheme is modelled with a single input and single output (SISO) method. Therefore, each matrix of Eq. (3) is a one-by-one or scalar matrix to formulate a SISO forecasting scheme-based-MPC modelling. This implies that $\forall k \in \mathbb{N} \Leftrightarrow A = [1]$, $B(k) = [\eta_{inv} p_{re}(k) \Delta k]$, $B_v(k) = B(k)$, $C = A$, $u(k) = P_{DC}(k)$ and $x(k) = c(k)$, with η_{inv} is the inverter efficiency, p_{re} is the real-time electricity price from the solar PV, P_{DC} is the generated DC power from the PV system, Δk is the time variation between k and $k-1$, and c is the cost of energy. Furthermore, DR programs offer several applications, including dynamic pricing, incentive programs, and automated DR. The dynamic pricing program contains real-time, time-of-use, and critical peak pricing schemes. Therefore, dynamic pricing-based real-time electricity pricing suggests an opportunity for the DSO to implement it regardless of the type of end-users

The system design, as presented in Eq. (3), is modelled by the function of the system state related to the energy cost from the PV plant and the dynamic of the energy market attached to the input matrix. Fig. 5 presents the dynamic implementation of the developed MPC-based-DR under a time-based program using a real-time pricing scheme

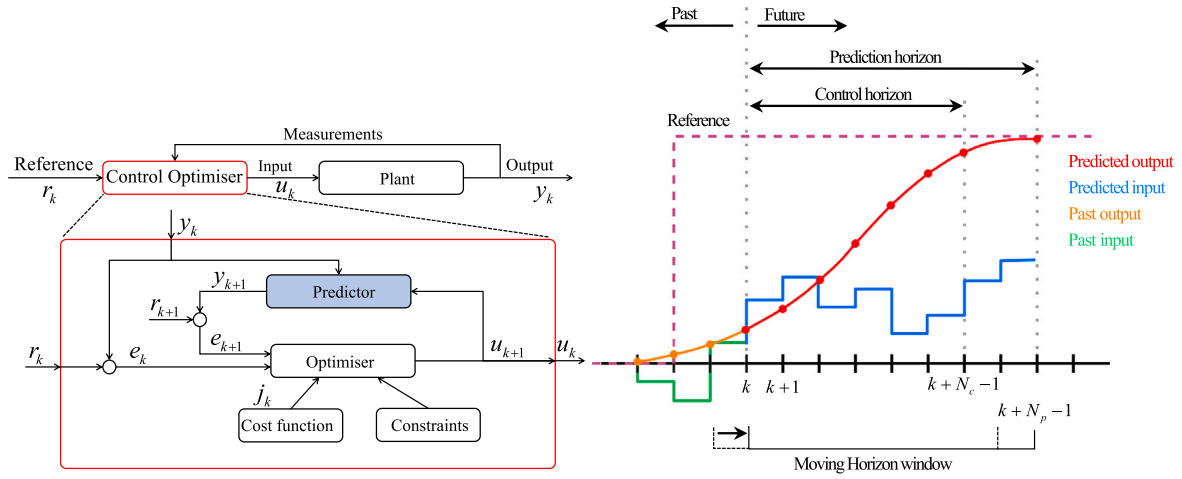

(a) Control loop. (b) Receding horizon.

Fig. 4. MPC: Implementation based-closed loop optimal control scheme [42].

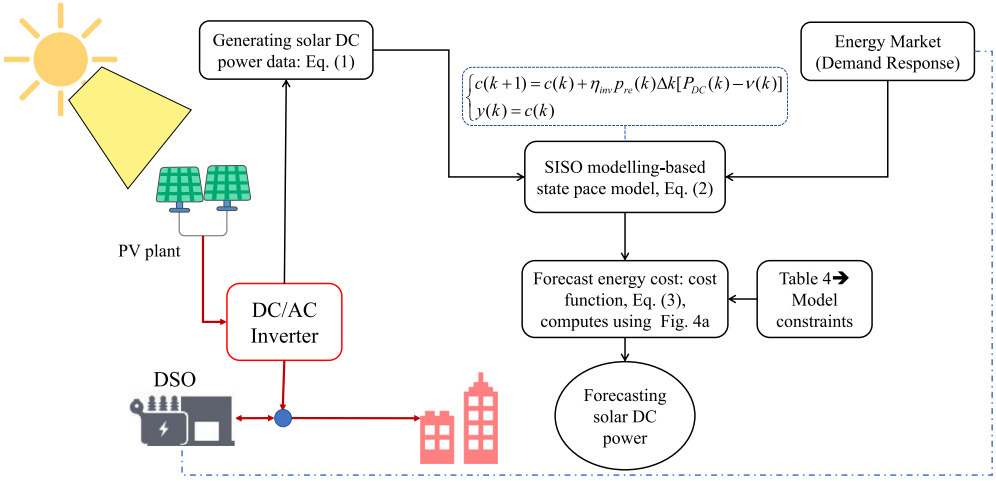

Fig. 5. Flowchart: SISO MPC modelling for solar power forecasting.

for DC solar power forecasting. This model only considers the dynamic electrical variable of the implementation configuration presented in Fig. 2, as summarized in Table 3. It should be hypothesized that the developed forecasting model interacts with the distributed system operator (DSO) only in the context of a real-time pricing scheme. Therefore, the load demand is not considered, and the forecast strategy assists in the optimal estimation of solar PV to be injected into the DSO.

By considering the closed-loop implementation model of the MPC, described in Fig. 4(a), the cost function of the MPC modelling developed in Eq. (3) is a quadratic shape as described in Eq. (4).

$$j(k) = (y(k) - r_w r(k))^T (y(k) - r_w r(k)) \tag{4}$$

with $r(k)$ and r_w are the reference or target to follow and turning parameter. As presented in Fig. 4(b) and detailed in Fig. 4(a), the implementation of this MPC approach is considered to optimally determine the input vector from Eq. (4). This process derives from the closed-loop approach presented in Fig. 4(a). An MPC is optimally computed through a moving horizon window procedure to determine optimal results of both future input and output signals at each sampling of time. Thus, the optimum output of the system in the function of the input signal is formulated as stated below:

$$y(k) = Fx(k) + \Phi(k)u(k) \tag{5}$$

Table 4
Summary of constraints matrix.

Constraint	Type	MPC	Equation
Input or control variable	Inequality	✓	$u_{min} \leq u \leqslant u$
Increment of control variable	Inequality	✓	$\Delta u_{min} \leq \Delta u \leqslant \Delta u$
Output or manipulated variable	Inequality	✓	$y_{min} \leq y \leqslant y_{max}$
State vector	Inequality	✓	$x_{min} \leq x \leqslant x_{max}$

with $F(k) = \begin{bmatrix} CA & CA^2 & \cdots & CA^{N_p} \end{bmatrix}^T$, and

$$\Phi(k) = \begin{bmatrix} CB(k) & 0 & \cdots & 0 \\ CAB(k) & CB(k) & & 0 \\ \vdots & \vdots & \ddots & \vdots \\ CA^{N_p-1}B(k) & CA^{N_p-2}B(k) & \cdots & CA^{N_p-N_c}B(k) \end{bmatrix}.$$

Eq. (6) presents a generalized formulation of the cost function of a quadratic function for the developed SISO MPC scheme for solar power forecasting, as demonstrated in Fig. 5. This model is fully constrained using the system constraints as detailed in Table 4. Therefore, the dynamic of MPC design can effectively be used to predict or forecast the DC power of solar PV plants. The advantage of this developed model-based forecasting method is its ability to have an intrinsic dynamic and handle various constraints of the system. Besides, the MPC implementation uses a quadratic optimization approach to compute the algorithm

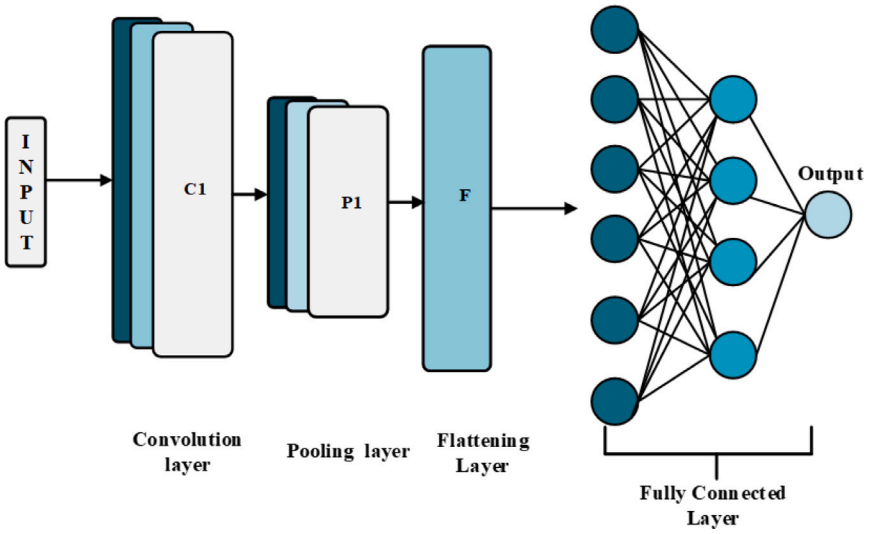

Fig. 6. 1D CNN strategy.

of the developed optimal control for the developed solar PV forecast, as presented in Fig. 5 [43].

$$J(k) = f(P_{DC}(k), r(k), p_{re}(k), r_w, N_c, N_p) \tag{6}$$

3.2. Convolutional neural network

CNNs are a prominent DL model widely used in image interpretation, video analytics, and classification due to their effective feature extraction and weight distribution capabilities. The study highlights CNN's recent success in time series analysis, particularly in voice automation recognition and wind speed forecasting.

CNNs differ from standard neural networks mainly due to their convolutional layers, which identify key features in the input data, aiding in understanding the relationship between the input and output variables. Thus, the CNN architecture comprises four main layers: pooling, flattening, convolutional, and fully connected layers, each serving a specific goal, as illustrated in Fig. 6.

Convolution procedures within the convolutional layer acquire characteristics from the input information. The pooling layer then aggregates these features, reducing dimensionality and enabling further feature extraction. The flattening layer converts the multi-dimensional feature maps from the pooling stage into a one-dimensional (1D) array, preparing them for the fully connected layer. Eventually, the regression prediction is performed by the completely connected layer, integrating the characteristics from the pooling and flattening stages.

For time series forecasting tasks, 1D convolutional filters are preferred. The convolutional layer operation is expressed as:

$$f = \Psi(\Omega^K * x + \beta^k) \tag{7}$$

where Ω represents the kernel weight factors, K is the number of kernels, x is the input series vector, β is the bias vector, $*$ denotes the convolution operation, and Ψ is the activation function. This study uses the rectified linear unit (ReLU) activation function to enhance computational efficiency for nonlinear data. The ReLU function is mathematically represented as:

$$\Psi(z) = \max(0, z) \tag{8}$$

where Ψ operates on the input z, applying a threshold operation that outputs the input itself when it is positive and zero when it is negative. This functionality enables the function to maintain linearity for non-negative values while providing a simple non-linear transformation for

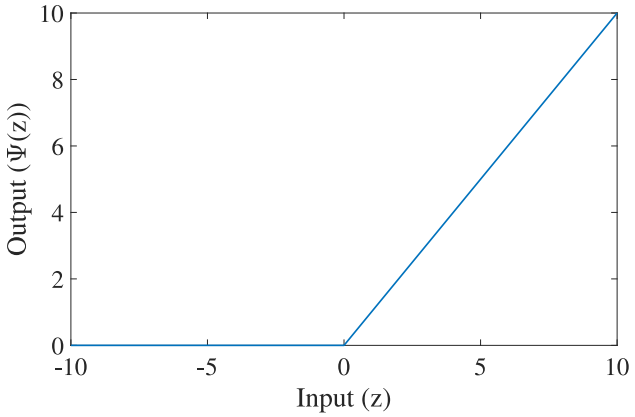

Fig. 7. ReLU activation function.

negative values, turning them to zero, as shown in Fig. 7. This characteristic is particularly beneficial as it helps in reducing the likelihood of the vanishing gradient problem and accelerates convergence during training.

After convolution, the feature dimension can be large. To reduce feature dimensions, a pooling layer follows the convolution layer. Maximum pooling is often more effective than average pooling for time series prediction, so this study uses maximum pooling. The maximum pooling operation is represented by:

$$Y_{\text{pool}} = \text{Pool}_{\max}(Y_{\text{conv}}) \tag{9}$$

In this operation, $\text{Pool}_{\max}$ scans through the feature map Y_{conv}, produced by the convolution layers, and methodically extracts the maximum value from each segment within the feature map. Each extracted maximum value signifies the most significant feature in that segment, effectively preserving only the strongest and most relevant features while discarding the less significant ones. Consequently, Y_{pool}, the output from the pooling layer, represents a condensed version of the input, where only the most critical information is retained.

In this work, a 1D CNN is utilized to predict the DC power of a PV system. Thus, the CNN procedure consists of two convolution layers, followed by a max pooling layer and, finally, a fully connected layer. The 1D CNN parameters are summarized in Table 5.

Table 5
Models parameters.

Model	Layer	Parameter	Value
CNN	Conv 1D (1)	Activation	Relu
		Filters	16
		Kernel size	3
	Conv 1D (2)	Activation	Relu
		Filters	32
		Kernel size	3
	Maxpooling	Pool size	2
	Fully connected 1	Number of units	50
		Activation	Relu
	Fully connected 2	Number of units	1
		Activation	linear
RF	–	Number of trees	100
		Max Depth	2
CNN-RF	Conv 1D (1)	Activation	Relu
		Filters	16
		Kernel size	3
	Conv 1D (2)	Activation	Relu
		Filters	32
		Kernel size	3
	Maxpooling	Pool size	2
	RF	Number of trees	100
		Max Depth	30

3.3. Random forest

RF, which was first introduced in 2001 by Breiman and further developed by XU in 2013, is considered one of the most popular ensemble approaches in ML [44]. This method incorporates the prediction capability of several decision trees to perform higher precision and resilience.

In RF, each decision tree is exposed to various subsets of the data through bootstrap sampling. This approach ensures that the trees learn differently and enhances their understanding of complex data.

Another interesting feature of RF is its randomized feature selection strategy. Instead of considering all features for every decision split, only a random subset is evaluated. This systematic approach helps prevent biases and excessive emphasis on features resulting in the generalization of the model.

The out-of-bag assessment procedure used by RF serves as an example of its reflective nature. Unlike machine learning models that rely on validation sets, RF internally validates itself. It uses data points excluded during bootstrap sampling to assess its performance continuously. This self-assessment allows the model to identify weaknesses and improve accuracy over time.

The insights obtained from decision trees are cleverly integrated within RF. The system uses either an averaging method or a voting system, depending on whether it is a task of predicting values or classifying data, as shown in Fig. 8. Therefore, it is essential to note that the ensemble design naturally reduces the chances of overfitting and guarantees the model's dependability. Due to the features mentioned earlier, in this study, the RF is employed to forecast the DC power of PV systems as a stand-alone model. The parameters that are used in RF are available within Table in Sub- Section 3.4.

The process of training a forest can be outlined in the subsequent steps:

1. Extract subsets of data from the dataset using Bootstrap Sampling.
2. Let a decision tree grow for each subgroup. A random subset of features is employed at each decision point in the tree to calculate the split.
3. Repeat the aforementioned steps until the forest reaches its desired size.
4. When new data is encountered, combine the predictions from trees by either averaging them for regression or using majority voting for classification to obtain the output of the random forest.

3.4. Hybrid convolutional neural network and random forest

In this study, a hybrid model named CNN-RF is also developed by integrating a 1D-CNN with the RF model. The main goal of this hybrid approach is to forecast the DC power output of a solar PV system. The CNN-RF architecture operates sequentially: the CNN functions as a sophisticated feature extractor, particularly suited for time series data. At the same time, the RF model utilizes these extracted features for the final prediction. The 1D structure of the CNN is ideal for uncovering hidden patterns within the temporal data, as its convolutional kernel operates in a unidirectional manner. Once these features are extracted, they are passed to the RF model, which acts as the regression mechanism to predict the output power of the PV plant. This serial combination allows the hybrid model to capitalize on CNN's ability to process raw, structured data and the RF's strength in delivering robust and accurate predictions.

The CNN architecture comprises two convolutional layers, a max pooling layer and a flattened layer, depicted in Fig. 9. The initial convolution layer processes the input sequence to generate feature maps. The following convolution layer manipulates these feature maps to produce additional maps. The max-pooling layer then compresses these maps, retaining only the most significant signal values. After pooling, the compressed data is flattened into a one-dimensional vector by the flattened layer. This step is essential as it transforms the sequential features extracted by the CNN into a format that can be fed into the RF model. The RF model then predicts the output power of the PV plant. Besides, the parameters utilized in the CNN-RF model are summarized in Table 5.

3.5. Hybrid recurrent neural network

A combination of BiLSTM and GRU is developed to mimic the DL strategy. This proposed architecture is applied for effective solar power prediction. The training and validation routines are used to account for and analogize the model. The LSTM network resolved the gradient explosion issue by permitting memory cells in the hidden layers. Therefore, these memory cells are employed to accumulate information appropriately. The LSTM's basic architecture is shown in [36]. Each cell of the LSTM consists of a forget gate (F_t), input gate (I_t) and output gate (O_t), which are used to tolerate or discard any information in each cell of LSTM architecture. For a forward movement function, the previous cell state 'C_{t-1}' has been discarded by the network. Therefore, the LSTM network should have three inputs: solar power P_t, the output of the previous memory cell (H_{t-1}), and the bias of the forget gate (B_F). As a result, the activation values can be written as:

$$F_t = \sigma\left(W_f\left[h_{t-1}, P_t(t)\right] + b_F\right) \tag{10}$$

Therefore, the final output of the memory cell can be formulated as follows:

$$O_t = \sigma\left(W_0\left[h_{t-1}, P_t(t)\right] + b_0\right) \tag{11}$$

$$H_t = \tanh(C_t) \tag{12}$$

where σ is a sigmoid function ranging from '0' to '1'; W_f and W_0 are weight vectors of the LSTM network; b_0, and b_F are bias vectors of the LSTM network.

3.5.1. Bi-directional long short-term memory

In the BiLSTM network, the underlying patterns and properties of data are captured via processing in both directions, which LSTM often disregards. The BiLSTM network is made up of a forward layer (F_l) and a backward layer B_l, allowing data to be processed both forward and backward [12]. In the BiLSTM network, the output sequence, the forward hidden layer and the backward hidden layer are utilized to update the network. The network iteratively updates from "T" to "1"

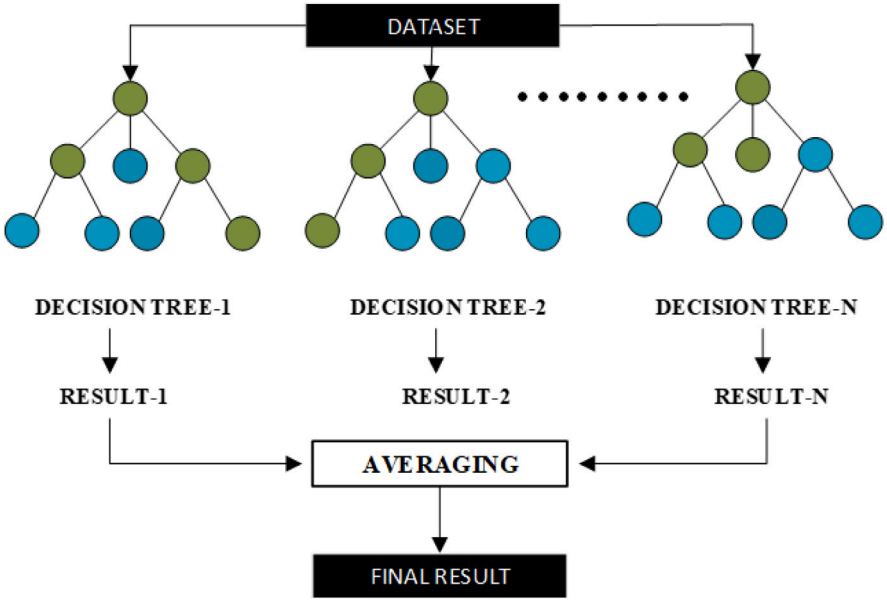

Fig. 8. Graphical representation of RF.

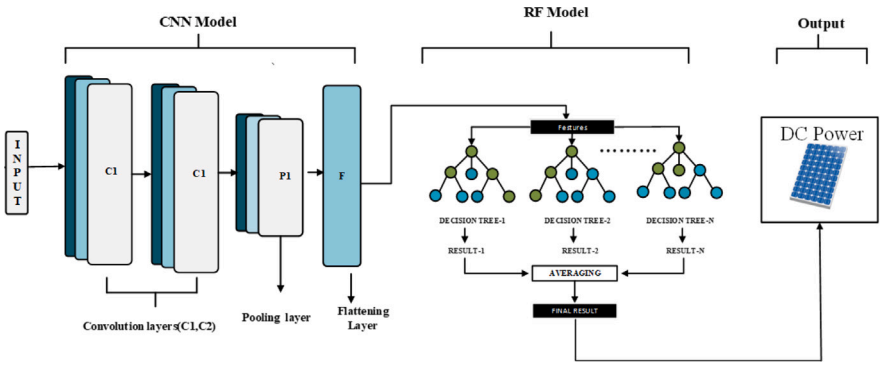

Fig. 9. Proposed Method: CNN-RF.

in the backward direction and from "1" to "T" in the forward direction. The parameters of the BiLSTM network are written below:

$$F_l = \sigma\left(W_1 P_i(t) + W_2 F_{l-1} + b_{F_l}\right) \tag{13}$$

$$B_l = \sigma\left(W_3 P_i(t) + W_5 B_{l-1} + b_{F_l}\right) \tag{14}$$

$$P_0 = \left(W_4 F_l + W_6 l + b_{P_0}\right) \tag{15}$$

with W is the weights coefficient, and P_0 is final output layer; and b_{F_l}, b_{B_l} and b_{P_0} are the biases [45].

3.5.2. Modified gated recurrent unit

In the suggested approach, the gated RNN-based GRU is formulated on BiLSTM to enhance the performance of the forecast strategy. GRU incorporates the LSTM's forget gate and input gate in a single update gate. Based on the fundamental layout of GRU architecture, Eq. (16) to (19) described the mathematical modelling of the developed architecture-modified GRU. Eq. (17) to (19) display the general equations of the GRU cell. In this model, the utilization of a stacked layer GRU is preferable due to its faster training with fewer parameters. Therefore, the framework is exemplified via Eqs. (16)–(18).

$$up_t = \sigma\left(w_{up}\left[h_{t-1}, Xi_t\right] + b_{up}\right) \tag{16}$$

$$r_t = \sigma\left(w_r\left[h_{t-1}, Xi_t\right] + b_r\right) \tag{17}$$

$$ac_t = \tanh\left(r_t w_{ac}\left[h_{t-1}, Xi_t\right] + b_{ab}\right) \tag{18}$$

$$h_t = (1 - up_t)ac_t + up_t h_{t-1} \tag{19}$$

where up_t is the updated gate, r_t is the reset gate, w_{up} is the weighted bias update gate, w_r is the weighted bias of the reset gate, Xi_t is the input data from the training set at time t, ac_t is the activation vector, h_t is the result of the output of the recent layer at time t, and b_{up} and b_r are the cell biases.

3.5.3. Hybrid BiLSTM-GRU

In this hybrid strategy, the possessions of DL techniques are utilized to develop a hybrid BiLSTM-GRU network, as illustrated in Fig. 10. It involves BiLSTM and multiple layers of GRU with a drop-out layer. This model offers adaptable complexity, leading to more effective training of input data with lower performance errors compared to fusion models found in the existing literature. Drop-out layers are included in the algorithm structure to mitigate data overfitting. The drop-out layer deactivates specific neurons during the training process. Therefore, BiLSTM strategies incorporate a drop-out layer between the BiLSTM and GRU layers. The model uses a sequence input layer, a BiLSTM layer with 500 hidden neurons, and two GRU layers with 200 hidden neurons. The probability of the drop-out layer is fixed at 0.1, and a completely connected layer is employed to obtain optimal forecasted outcomes.

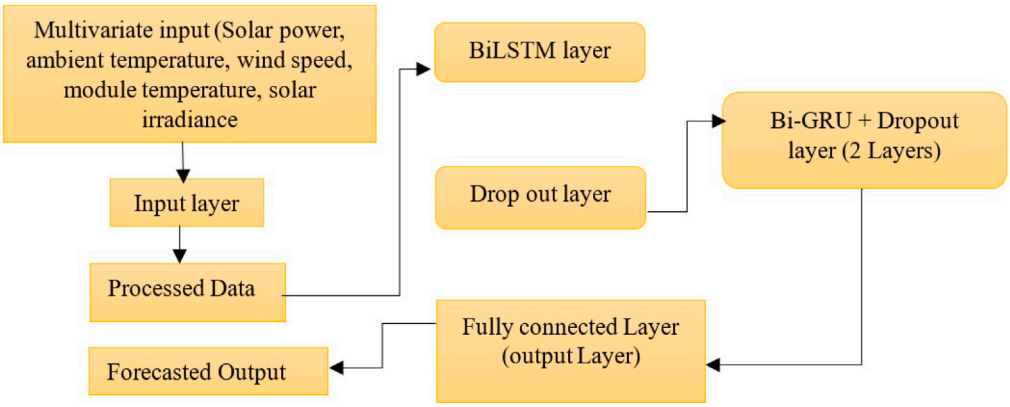

Fig. 10. Hybrid RNN-based BiLSTM and GRU Model.

3.6. Forecasting assessment: Evaluation metrics

Some relevant evaluation metrics are selected to assess the performance of the developed forecasting benchmarks for the solar PV power output. The reverent metrics recommended by studies and reports in the field have been selected. The chosen metrics include R-squared (R^2), mean square error (MSE), root mean square error (RMSE), and mean absolute error (MAE) [36]. RMSE is commonly used as an evaluation metric in forecasting studies because it effectively penalizes significant errors. MAE illustrates the difference value of the forecasted and reference DC solar power values, providing a comprehensive overview of how closely the predictions match the actual measurements. R^2, also referred to as the determination coefficient, estimates the variation proportion in the dependent variable that the independent variables can illustrate. Its values range between 0 and 1 (or 0% to 100%), with a value approaching 1, signifying that the model possesses a high predictive accuracy and closely corresponds with the observed data. The formulations for these metrics are as follows:

$$R^2 = 1 - \frac{\sum(y_i - \hat{y}_i)^2}{\sum(y_i - \bar{y}_i)^2} \tag{20}$$

$$MSE = \frac{1}{N}\sum_{i=1}^{N}(y_i - \hat{y}_i)^2 \tag{21}$$

$$RMSE = \sqrt{\frac{1}{N}\sum_{i=1}^{N}(y_i - \hat{y}_i)^2} \tag{22}$$

$$MAE = \frac{1}{N}\sum_{i=1}^{N}|y_i - \hat{y}_i| \tag{23}$$

with N describes the total horizon of time steps, $\hat{y}_i$ is the forecasted output power from the PV plant, y_i denotes the reference power, $\bar{y}_i$ is the mean of the reference.

4. Results and discussion

The solar PV DC power forecast is implemented by applying predictive techniques [6], which are model-based MPC and four data-driven ML strategies. The four developed ML models are CNN, RF, CNN-RF, and DL-based hybrid BiLSTM-GRU. The implementation of CNN RF, CNN, CNN-RF, and BiLSTM-GRU is executed in Python, utilizing Jupyter Notebook. TensorFlow and KERAS served as the principal tools for DL, facilitating the assembly of models. For tasks related to data manipulation and processing, Sci-kit Learn and several fundamental Python libraries were employed. The results are presented for one week for each particular developed model. The system implementation of the developed models is validated using the specifications provided in Tables 2–5, depending on each design scheme. Each developed strategy is tested in two scenarios. In the first case, the validation of the design performance is tested without disturbance. The second scenario is validated by a disturbance from solar radiation during the second day of the week.

4.1. Scenario-1: Without disturbance

The model-based approach is a quadratic formulation of the MPC design developed in Eqs. (4)–(6) and depends on some of the most critical factors of the implementation process, including the dynamic of $p_{re}(k)$, N_c, N_p, r_w and system constraints, as described in Table 4. Thus, N_c and r_w play an essential role in determining a suitable performance index value at each sampling time as the computational system is required to handle the system constraints and a determined N_p. In this first case, $\forall k \in \mathbb{N} \Rightarrow v(k) = 0$, as developed in the model-based system in Eq. (3). Therefore, the system can be computed without input disturbance. Figs. 11(a) and 11(b) present the optimal forecasting results from the MPC scheme.

The system implementation of the MPC uses a variable N_c with a fixed N_p of one day, equivalent to a 288-data point. This implementation is based on the moving horizon window, as shown in Fig. 4(b). The r_w and N_c actively participate in the system performance. Thus, $\forall k \in \mathbb{N}$ if $r_w \leq 2 \Rightarrow$ the system performance is not suitable to predict optimum results. Two other r_w values, 2 and 2.5, have optimally been applied to validate the robustness of the MPC design. Besides, five specific points of time within the daily based on N_p are also set to identify the control horizon optimally, N_c. These are 12, 24, 36, 48, and 60, equivalent to the first, second, third, fourth, and fifth hours within a day. Table 6 presents the evaluation metrics of the MPC strategy in different horizon windows in the function of r_w and N_c, as depicted in Figs. 11(a) and 11(b).

Figs. 11(c)–11(f) respectively show the results from RF, CNN, CNN-RF, and BiLSTM-GRU data-driven strategies. Table 7 compares the performance of each ML method. Thus, it can be observed that each model optimally follows the reference. Additionally, it is observed that the error metrics are lower for the developed hybrid BiLSTM-GRU than those of other MLs and benchmark models in the literature, with a 99% coefficient of regression [36]. Besides, in the literature, usually, the data was tested for 9:1, 8:2, or 7:3 ratios [12,46]; the developed BiLSTM-GRU model in this study is tested for data in the ratio 5:5 training and testing data, and the results have been shown only for seven days to validate the developed hybrid BiSLT-GRU architecture. Moreover, the hybrid CNN-RF method demonstrates superior performance in multivariate data analysis to predict solar power.

It is observed that for $r_w \geq 2.5$ and $N_c \geq 48$, the MPC strategy predicts satisfactory results. For ML strategies, as shown in Table 7, the best-performed model is the CNN-RF, with the lowest RMSE at 14.276, MSE at 203.806, and MAE at 8.072. In addition, the CNN-RF achieved the preeminent R^2 value of 0.9996 compared to other data-driven strategies. In terms of performance, when considering RMSE, it

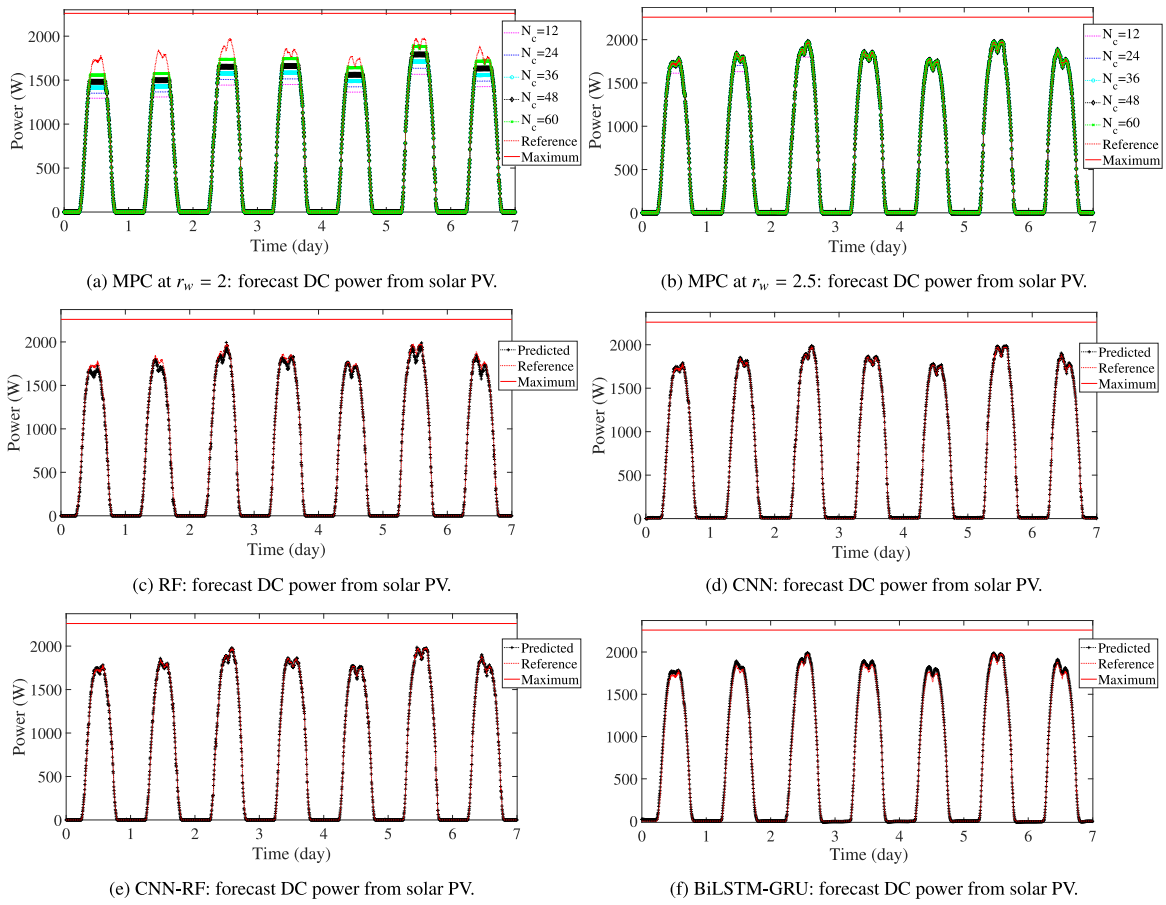

(a) MPC at r_w = 2: forecast DC power from solar PV.

(b) MPC at r_w = 2.5: forecast DC power from solar PV.

(c) RF: forecast DC power from solar PV.

(d) CNN: forecast DC power from solar PV.

(e) CNN-RF: forecast DC power from solar PV.

(f) BiLSTM-GRU: forecast DC power from solar PV.

Fig. 11. DC solar PV power forecast without disturbance for the entire week.

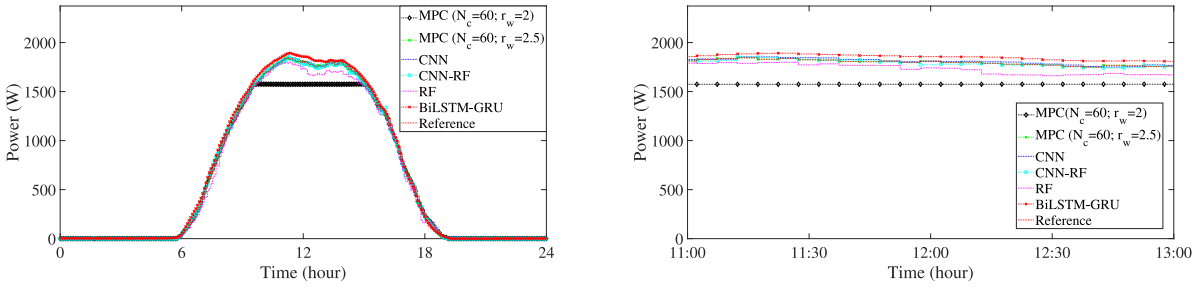

(a) For 24 hours.

(b) For 2 hours.

Fig. 12. DC solar PV power forecast without disturbance within a day.

can be seen that the inclusion of RF in CNN has roughly improved performance. On the other hand, the inclusion of CNN to RF has improved RF performance by approximately 19.527 W, which is above 50%. This can be attributed to the ability of CNN to extract complex features from the data. Thus, it can be concluded that the combination of CNN and RF has enhanced the predictive accuracy since it integrates the distinctive features of both models.

The CNN can be classified as the second ML strategy since it has, at best, R2, RMSE, and MAE, followed by RF and then BiLSTM-GRU. Besides, the hybrid BiLSTM-GRU also provides optimal results for a suitable solar DC power forecast prediction. Additionally, it is observed that the predicted values closely align with the observed values, as depicted in Figs. 11(c)–11(f), and the different performance metrics evaluation is given in Table 7.

Fig. 12 presents a profile prediction profile within a day for 24 h and 2 h of the most relevant MPC schemes based on N_c = 60 and r_w = 2 or 2.5, and all ML strategies to assess the system performance. This shows that when r_w < 2.5, the ML schemes perform better than the robustness of the MPC regardless of the optimal value of N_c, as described in Tables 6–7. It should also be adequate to mention the DR scheme dynamic has actively participated in the computational process robustness of the MPC design to forecast the solar DC power, as developed in Fig. 5.

4.2. Scenario-2: With disturbance

The second case considers an external disturbance from solar irradiation that affects the power generated by the PV systems. In this scenario, $\forall k \in \mathbb{N} \Rightarrow \nu(k) \neq 0$, as described in Eq. (3). Thus, an additional step of the system models is taken by incorporating data instabilities on irradiance data on the second day of the last 7 days, as depicted in Fig. 12. This instability is an outside disturbance for the system

Table 6
Performance Evaluation Criteria of MPC strategies without disturbance.

Criteria	MPC									
	$r_w = 2$					$r_w = 2.5$				
	$N_c = 12$	$N_c = 24$	$N_c = 36$	$N_c = 48$	$N_c = 60$	$N_c = 12$	$N_c = 24$	$N_c = 36$	$N_c = 48$	$N_c = 60$
R^2	0.939466	0.957701	0.973378	0.985864	0.994432	0.997765	0.99951824	0.999979	1	1
MSE (W)	36 484.88	25 494.42	16 045.38	8519.986	3355.9	1347.224	290.3627261	12.69	0	0
RMSE (W)	191.0101	159.6697	126.6704	92.30377	57.93013	36.70455	17.04003304	3.562303	0	0
MAE (W)	97.99967	79.60943	60.78194	41.66653	22.8534	11.53508	3.709537766	0.307871	0	0

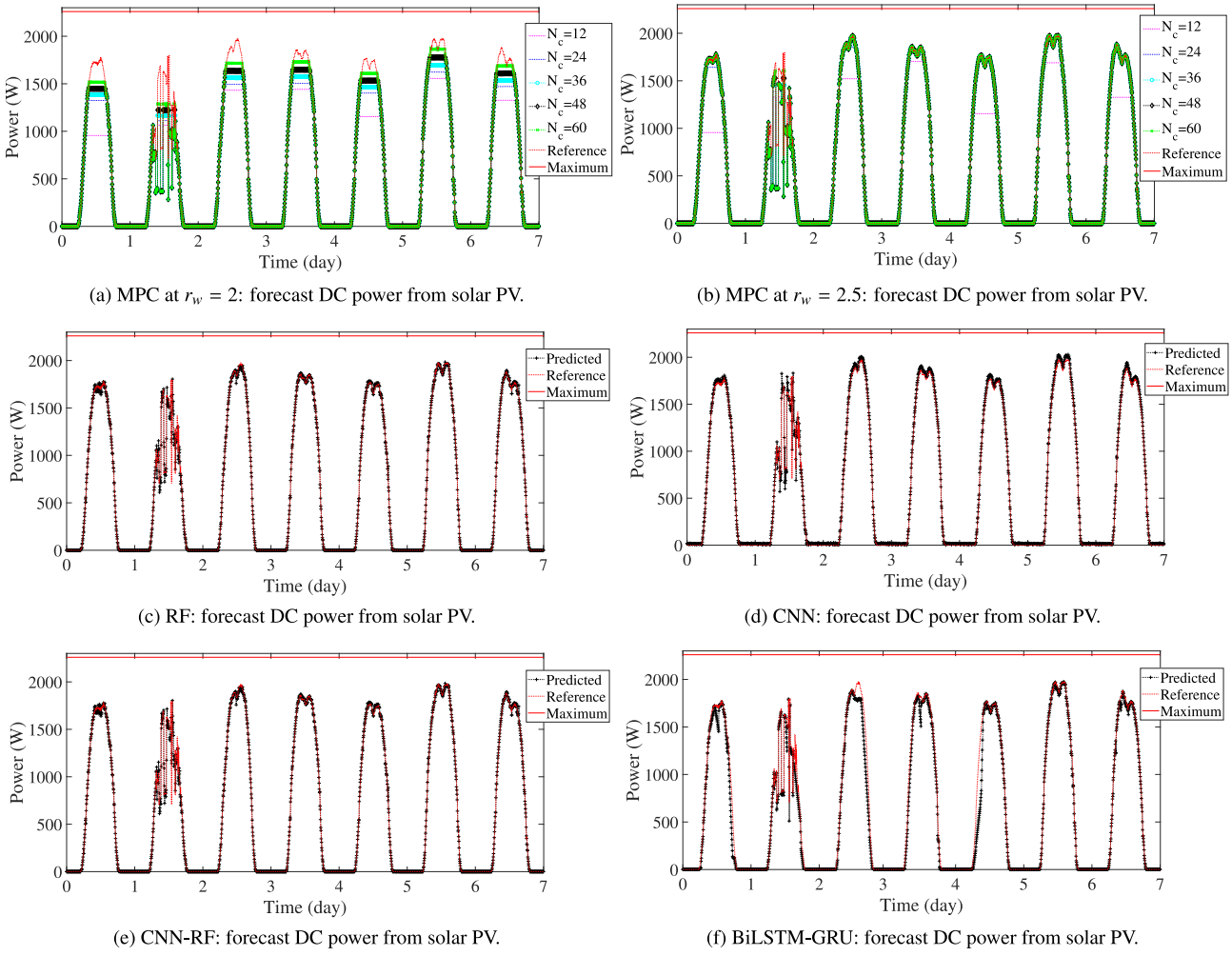

(a) MPC at $r_w = 2$: forecast DC power from solar PV.

(b) MPC at $r_w = 2.5$: forecast DC power from solar PV.

(c) RF: forecast DC power from solar PV.

(d) CNN: forecast DC power from solar PV.

(e) CNN-RF: forecast DC power from solar PV.

(f) BiLSTM-GRU: forecast DC power from solar PV.

Fig. 13. DC solar PV power forecast with disturbance for the entire week.

Table 7
Performance Evaluation Criteria of ML Strategies without disturbance.

Criteria	RF	CNN	CNN-RF	BiLSTM-GRU
R^2	0.9981	0.9994	0.9996	0.9980
MSE (W)	1142.211	316.803	203.806	1228.4
RMSE (W)	33.803	17.799	14.276	35.0483
MAE (W)	18.897	14.043	8.072	22.9366

models of solar power forecasting. As an external disturbance in the input variable of the system design, it has been observed that the solar power could be reduced by an external variable on the second day from a range of 40%–90%, and a deep ending on the irradiance data is added on the same day. The other input variables are equally interpreted according to these perturbations introduced in the solar irradiance data. The observed disturbance magnitude represents realistic variations in solar irradiance caused by factors like cloud cover, shading, or atmospheric changes, with the "deep ending" simulating extreme conditions such as sudden heavy cloud cover or approaching storms. The process of considering such disturbance to the observational data is carried out to verify that the developed models are robust with acceptable or suitable performance metrics, as developed in Eqs. (20)–(22). In operational meteorological models, this type of data synthesis is commonly used to generate significant variations in the data condition that will be used in subsequent forecasts. Thus, the results for each developed method are displayed in Fig. 13.

Figs. 13(a) and 13(b) present the results of MPC with the set optimal r_w when the system considers the disturbance into the input signal. The robustness of the MPC shows its consistency in handling the system constraints described in Table 4. However, it is observed that due to the disturbance in the input signal, the predicted power struggles to smoothly follow the system reference. This is compared with the optimal results from the MPC scheme during the first scenario, as presented in Figs. 11(a) and 11(b). In the second scenario, N_c and r_w

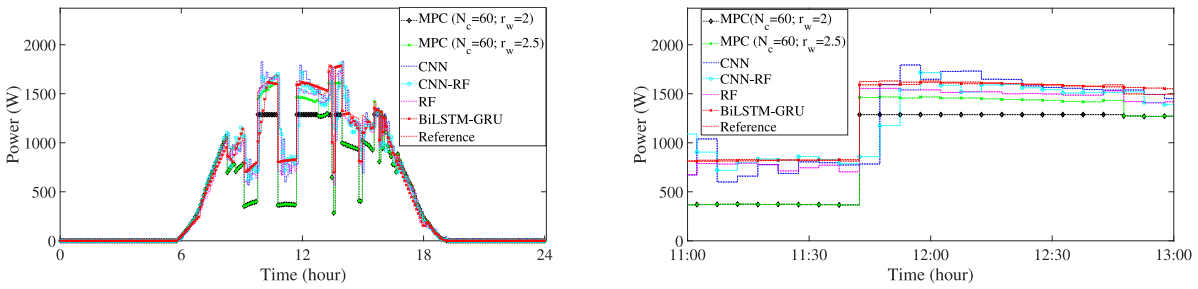

(a) For 24 hours. (b) For 2 hours.

Fig. 14. DC solar PV power forecast with a disturbance within a day.

Table 8
Performance Evaluation Criteria of MPC strategies with disturbance.

Criteria	MPC									
	$r_w = 2$					$r_w = 2.5$				
	$N_c = 12$	$N_c = 24$	$N_c = 36$	$N_c = 48$	$N_c = 60$	$N_c = 12$	$N_c = 24$	$N_c = 36$	$N_c = 48$	$N_c = 60$
R^2	0.88722	0.946601	0.96251	0.975578	0.98515	0.91157	0.99204	0.99325	0.99368	0.99393
MSE (W)	65 352.50	30 942.26	21 725.93	14 151.52	8603.36	51 240.21	4609.42	3905.78	3658.03	3516.64
RMSE (W)	255.6413	175.9041	147.3972	118.9601	92.7543	226.3630	67.8926	62.4963	60.4817	59.3013
MAE (W)	134.1686	89.4258	72.1779	54.6686	37.1700	109.2288	16.9865	12.9254	11.9905	11.5997

Table 9
Performance Evaluation Criteria of ML Strategies with disturbance.

Criteria	RF	CNN	CNN-RF	BiLSTM-GRU
R^2	0.99772	0.99407	0.99474	0.9949
MSE (W)	1319.9553	3442.1238	3050.6081	2980,0
RMSE (W)	36.3312	58.6693	55.2323	54.6067
MAE (W)	20.2126	27.7898	16.3711	16.896

also play the same role in optimal PV system power prediction. The data-driven strategies, including RF, CNN, CNN-RF and BiLSTM-GRU, present predicted profiles that asymptotically follow the reference, as presented in Figs. 13(c)–13(f). The same behaviours can be observed throughout model-based-MPC assessment when $r_w \geq 2.5$ and $N_c \geq 24$, as depicted in Fig. 13(b). Besides, Fig. 13(f) shows that the predicted power from the hybrid BiLST-GRU stumbles from following the reference when the disturbance is considered compared to the undisturbed model, as shown in Fig. 11(f). An effective comparison between the first and the second scenarios can demonstrate the robustness of the developed model-based and data-driven-based strategies. This can be assessed by Fig. 11 compared to Fig. 13. For the CNN-RF, the result presented in Fig. 13(e) shows an optimal following of the reference. The non-hybrid schemes, RF and CNN, also present optimal predictions when the disturbance is considered, as depicted in Figs. 13(c) and 13(d).

Fig. 14 demonstrates the effectiveness of the suggested models to forecast the generating power from the PV plan during the disturbance. For the MPC, with $N_c = 60$ and $r_w = 2$ or 2.5, the results demonstrate that the approach under-predicted the generated power during the disturbance. Besides, Fig. 12 presents the under-prediction of the MPC implementation when $r_w = 2$, as also shown in Figs. 11(a) and 13(a). Nevertheless, the under-prediction for the MPC scheme can be caused by several factors and variables, such as the dynamic behaviour of the designing model, the system constraints formulated in Table 4, N_c and r_w as shown in Fig. 11(a). ML strategies also show optimal results throughout the disturbing day, as presented in Fig. 14. A slight over-prediction has been observed throughout the disturbing period for each ML scheme. The data-driven methods are also affected by a slight underestimation of the forecast power from the PV system. In 12, this over and under-prediction can be considered negligible for ML strategies. Besides, Tables 6–9 can considerably assist in evaluating the impact of over and under-predictions for each approach.

4.3. Discussion

It can be observed in Figs. 11 and 14 that the DC power predicted by the proposed models closely matches the reference DC power. It is important to note that these profiles do not provide a reliable reference for model comparison between strategies and scenarios. Therefore, the evaluation metrics described in Section 3.6 are utilized to assess a comparative examination of the performance of various approaches, as shown in Tables 6–9. They can also provide a more thorough knowledge of the benefits of each method through optimal solar power forecasting modelling and an opportunity for a comprehensive comparative analysis of strategies during all operation conditions.

For instance, Figs. 13 and 14 are insufficient to show an effective discussion and comparison assessment of the system design. These profiles are summarized in Tables 8 and 9 for an effective evaluation of developed models based on the performance metrics of each strategy. Therefore, Fig. 15 provides a critical assessment based on a comparative of each method during both scenarios. Table 8 describes the assessment metrics of the MPC scheme while considering disturbance. For $r_w = 2$, the MPC scheme possesses the same performance without disturbance in terms of following the target, as shown in Figs. 11(a) and 13(a). Besides, their evaluation can be considered unsuitable for the optimal prediction of solar DC power from the PV plant compared to MPC (when $r_w \geq 2.5$) and all data-driven approaches. As shown in Table 8, the predicted values are optimal when $r_w \geq$=2.5. However, the results are less competitive from the effectiveness of the optimal values without disturbance, as presented in Table 7, especially for $N_c = 48$ or 60 with R^2=1 and MSE=RMSE=MAE=0. These differences in the performance of MPC strategies can also be observed in Figs. 15(a) and 15(b).

Amongst ML approaches, it is demonstrated that the hybrid BiLSTM-GRU provides certain great performance metrics compared to some MLs. This is regardless of its profile, as shown in Fig. 11(f). Thus, the hybrid BiLSTM-GU possess an excellent R^2, MSE, and RMSE than CNN and CNN-RF, as shown in Table 9. However, in the first scenario, performance metrics from the BiLSTM-GRU strategy could not be compared to the performance of all ML approaches, as demonstrated in Table 7. It can be observed that the over and under-prediction of BiLSTM-GRU, as depicted in Fig. 13(f), could play a significant role in providing some excellent performance metrics in the disturbed scenario. The most performing ML approach in the undisturbed implementation, as

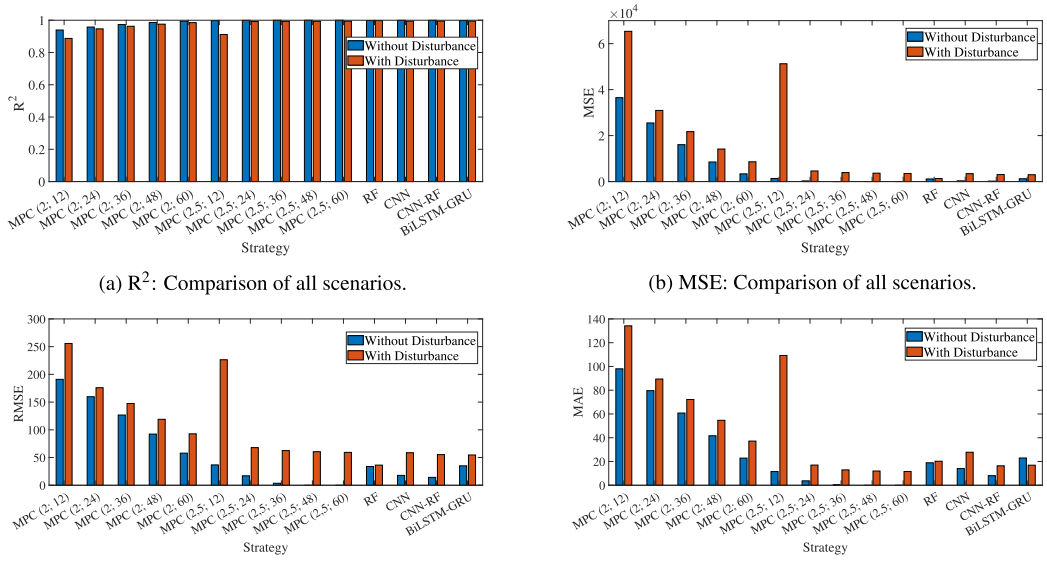

(a) R^2: Comparison of all scenarios.

(b) MSE: Comparison of all scenarios.

(c) RMSE: Comparison of all scenarios.

(d) MAE: Comparison of all scenarios.

Fig. 15. Performance metrics comparison: Undisturbed and disturbed assessment.

Table 10
Forecasting Methods: Assessment of the implemented strategies.

Methods	Observations	Advantages	Disadvantages	Comparison	Summary
MPC	– Intrinsic dynamic handling and constraint management in the prediction process enhance the forecast's reliability.	– Effective handling of constraints, real-time data optimization, and high control accuracy. - High scalability. - Optimal prediction.	– High computational complexity requires a model of the system and implementation cost. - Computational complexity is increasingly variable in function of the prediction horizon and system model elaborateness.	– More dynamic and constraint-aware than static methods like RF. - Scalable with advances in computational hardware and optimization techniques.	– A robust closed-loop control strategy optimizing future inputs and outputs for solar PV forecasting using a state-space model. - It is excellently suitable for real-time applications, including being viable for real-time control in large-scale PV systems, particularly with optimized configurations.
CNN	– CNN layers extract significant features, reducing dimensionality while preserving essential information. Maximum pooling effectively retains critical features for prediction..	– Efficient feature extraction and dimensionality reduction.	– Requires large datasets for training and can be computationally intensive.	–More efficient at feature extraction than traditional ML methods like RF.	–Uses convolutional and pooling layers to extract and condense features for accurate time series forecasting, particularly in predicting PV system DC power output.
RF	– RF's self-assessment through out-of-bag samples provides continuous validation, ensuring improved accuracy and model generalization.	– Robust to overfitting and handles complex datasets well. - High scalability.	– Can be less interpretable than simpler models and computationally intensive. - Moderate computational complexity, which is parallelisable and computationally efficient, depends on the number of trees and depth.	– More robust and generalizable than single decision trees. - Robust and scalable to large datasets and systems.	– Uses multiple decision trees to enhance precision and resilience in predictions, effectively generalizing the model to reduce overfitting, suitable for forecasting PV system DC power. - Excellent suitability in real-time systems, including low latency, highly suitable for real-time applications.

(*continued on next page*)

Table 10 (*continued*).

Methods	Observations	Advantages	Disadvantages	Comparison	Summary
CNN-RF	– CNN extracts significant time series features, which are then used by RF for accurate regression and prediction, improving overall forecasting performance.	– Combines strengths of CNN and RF for better performance. - Moderate scalability.	– Increased model complexity and computational requirements. - High computational complexity. This involves convolutional operations and random forest regression, requiring significant computational resources for training.	– Combines efficient feature extraction of CNN with robust regression of RF. - Suitable for medium-scale systems; may require optimization for larger systems.	– A hybrid model combining CNN for feature extraction and RF for regression, effectively predicting PV system DC power by leveraging both models' strengths. - Good suitability for real-time applications, fast inference once trained, suitable for real-time in medium-scale systems.
BiLSTM-GRU	– Combines the bidirectional processing of BiLSTM with the efficiency of GRU, enhanced by dropout layers to prevent overfitting, providing a robust model for accurate prediction.	– Combines strengths of BiLSTM and GRU with dropout to prevent overfitting. - Moderate to low scalability.	– Increased model complexity and computational requirements. - High computational complexity. This is caused by resource intensive due to the sequential processing of time series data, demanding training	– More robust and effective than using BiLSTM or GRU alone due to combined strengths and dropout. - Effective in variable conditions but may require optimization for large-scale systems.	– Combines BiLSTM and GRU, along with dropout layers, to enhance training effectiveness and prediction accuracy for complex sequential data, making it suitable for solar power forecasting. - Suitably moderate for real-time applications. This requires optimization for real-time use, especially in large systems.

presented in Section 4.1, was CNN-RF, with excellent performance metric values compared to all ML methods. Table 9 shows that the RF method is the best-performing model, with exceptional R^2, MSE and RMSE, followed by BiLSTM-GRU, CNN-RF and CNN.

Moreover, as presented in Figs. 15(a)–15(d), RF provides a robust forecast behaviour with less difference between performance metrics of the disturbed and undisturbed methods. It can be glanced that the addition of CNN did not enhance the performance of the RF model. However, including RF in CNN has slightly improved the performance of CNN-RF, especially when evaluating MAE, as shown in Fig. 15(d), compared to all ML strategies during the disturbed scenario. Thus, as shown in Fig. 13 and Table 9, if only MAE is considered as the best suitable criterion to evaluate the most performing approach, this should be the MPC with $r_w = 2.5$ and $N_c \geq 48$, followed by CNN-RF, BiLSTM-GRU, RF and CNN. Therefore, the determination of a suitable solar PV power forecast model, either model-based or model-free strategy, depends on data structure, disturbance, and system configuration and modelling, including parameters, location, and constraints.

It has been observed that considering the computational complexity and scalability of each method is essential to providing further insights into the practicality of these forecasting approaches for real-time applications and their potential scalability to larger PV systems. Thus, Table 10 summarizes these aspects of the discussed and developed models, including the computational complexity, scalability and suitability for real-time applications.

5. Conclusion

In this paper, an MPC under the DR scheme for predicting the DC power production of solar PV systems is developed. This method is compared to various data-driven models, including RF, CNN, CNN-RF and BiLSTM-GRU strategies. The models were tested using real-time data from the University of Sharjah solar power plant in Sharjah, UAE, with data normalization techniques used to improve the training algorithms for each machine-learning scenario. The obtained results demonstrate that the main goal of accurately forecasting the DC power of the PV system using MPC under the DR system has been achieved. The DR scheme provides a dynamic opportunity to support the robustness of the computational process of the MPC design for effective solar DC power forecasting. Therefore, the MPC strategy offers an excellent and accurate power forecast with the best evaluation metrics compared to ML approaches during the undisturbed scenario. This shows that MPC is robust compared to selected ML approaches. For ML strategies, the hybrid of CNN-RF provides better results than other data-driven schemes. The hybrid BiLSTM-GRU is regarded as the last in the list of all developed ML approaches. Moreover, if an external disturbance is considered, MPC provides optimal results with some lower performance metrics values compared to all ML approaches. RF is regarded as a suitable model with best-performance metrics when the disturbance is considered. Therefore, this work offers an opportunity to accelerate and improve the precision and utilization of energy resource planning. Furthermore, each developed model of this work can effectively be used to predict and assess an accurate energy resource.

Future studies will also look at implementing the developed model at the tertiary control level of microgrids for optimal energy coordination. This will serve as an opportunity to create a digital twin model for optimum solar power plants to guarantee the total load demand and net-zero vision.

CRediT authorship contribution statement

Nsilulu T. Mbungu: Writing – review & editing, Writing – original draft, Visualization, Validation, Supervision, Software, Resources, Project administration, Methodology, Investigation, Funding acquisition, Formal analysis, Data curation, Conceptualization. **Safia Babikir Bashir:** Writing – review & editing, Writing – original draft, Visualization, Validation, Software, Resources, Methodology, Investigation, Funding acquisition, Formal analysis, Data curation. **Neethu Elizabeth Michael:** Writing – review & editing, Writing – original draft, Visualization, Validation, Software, Resources, Methodology, Investigation, Funding acquisition, Formal analysis, Data curation. **Mena Maurice Farag:** Writing – review & editing, Writing – original draft, Visualization, Validation, Investigation, Formal analysis, Data curation. **Abdul-Kadir Hamid:** Writing – review & editing, Visualization, Validation, Supervision, Methodology, Investigation, Funding acquisition, Formal analysis. **Ali A. Adam Ismail:** Writing – review & editing, Writing – original draft, Visualization, Validation, Supervision, Methodology, Investigation, Funding acquisition, Data curation. **Ramesh C. Bansal:** Writing – review & editing, Visualization, Validation, Software, Resources, Methodology. **Ahmed G. Abo-Khalil:** Writing – review & editing, Visualization, Validation, Methodology, Investigation, Formal analysis. **A. Elnady:** Writing – review & editing, Visualization, Validation, Methodology, Investigation, Funding acquisition, Formal analysis.

Mousa Hussein: Writing – review & editing, Visualization, Validation, Methodology, Investigation, Formal analysis, Data curation.

Declaration of competing interest

The authors declare that they have no known competing financial interests or personal relationships that could have appeared to influence the work reported in this paper.

Data availability

Data will be made available on request.

References

[1] Hamid AK, Mbungu NT, Elnady A, Bansal RC, Ismail AA, AlShabi MA. A systematic review of grid-connected photovoltaic and photovoltaic/thermal systems: Benefits, challenges and mitigation. Energy Environ 2022;0958305X221117617.

[2] Sarkodie SA. Winners and losers of energy sustainability—Global assessment of the sustainable development goals. Sci Total Environ 2022;831:154945.

[3] Hunter CA, Penev MM, Reznicek EP, Eichman J, Rustagi N, Baldwin SF. Techno-economic analysis of long-duration energy storage and flexible power generation technologies to support high-variable renewable energy grids. Joule 2021;5(8):2077–101.

[4] O'Malley M, Bowen T, Bialek J, Braun M, Cutululis N, Green T, et al. Enabling power system transformation globally: A system operator research agenda for bulk power system issues. IEEE Power Energy Mag 2021;19(6):45–55.

[5] Jayachandran M, Gatla RK, Rao KP, Rao GS, Mohammed S, Milyani AH, et al. Challenges in achieving sustainable development goal 7: Affordable and clean energy in light of nascent technologies. Sustain Energy Technol Assess 2022;53:102692.

[6] Mbungu NT, Ismail AA, AlShabi M, Bansal RC, Elnady A, Hamid AK. Control and estimation techniques applied to smart microgrids: A review. Renew Sustain Energy Rev 2023;113251.

[7] Zheng W, Lu H, Zhang M, Wu Q, Hou Y, Zhu J. Distributed energy management of multi-entity integrated electricity and heat systems: A review of architectures, optimization algorithms, and prospects. IEEE Trans Smart Grid 2023.

[8] Farag MM, Bansal RC. Solar energy development in the GCC region–a review on recent progress and opportunities. Int J Modelling Simul 2023;43(5):579–99.

[9] Wang X, Lu Z, Li T, Zhang P. Carbon-neutral power system transition pathways for coal-dominant and renewable resource-abundant regions: Inner Mongolia as a case study. Energy Convers Manage 2023;285:117013.

[10] Ayoub M. 100 years of daylighting: A chronological review of daylight prediction and calculation methods. Sol Energy 2019;194:360–90.

[11] Kamadinata JO, Ken TL, Suwa T. Sky image-based solar irradiance prediction methodologies using artificial neural networks. Renew Energy 2019;134:837–45.

[12] Michael NE, Hasan S, Al-Durra A, Mishra M. Short-term solar irradiance forecasting based on a novel Bayesian optimized deep long short-term memory neural network. Appl Energy 2022;324:119727.

[13] Poti KD, Naidoo RM, Mbungu NT, Bansal RC. Optimal hybrid power dispatch through smart solar power forecasting and battery storage integration. J Energy Storage 2024;86:111246.

[14] Ahmad T, Madonski R, Zhang D, Huang C, Mujeeb A. Data-driven probabilistic machine learning in sustainable smart energy/smart energy systems: Key developments, challenges, and future research opportunities in the context of smart grid paradigm. Renew Sustain Energy Rev 2022;160:112128.

[15] Das UK, Tey KS, Seyedmahmoudian M, Mekhilef S, Idris MYI, Van Deventer W, et al. Forecasting of photovoltaic power generation and model optimization: A review. Renew Sustain Energy Rev 2018;81:912–28.

[16] Sobri S, Koohi-Kamali S, Rahim NA. Solar photovoltaic generation forecasting methods: A review. Energy Convers Manage 2018;156:459–97.

[17] Farag MM, Hamid A-K, AlMallahi MN, Elgendi M. Towards highly efficient solar photovoltaic thermal cooling by waste heat utilization: A review. Energy Convers Manage 2024;100671.

[18] Poti KD, Naidoo RM, Mbungu NT, Bansal RC. Intelligent solar photovoltaic power forecasting. Energy Rep 2023;9:343–52.

[19] Benali L, Notton G, Fouilloy A, Voyant C, Dizene R. Solar radiation forecasting using artificial neural network and random forest methods: Application to normal beam, horizontal diffuse and global components. Renew Energy 2019;132:871–84.

[20] Munsif M, Ullah M, Fath U, Khan SU, Khan N, Baik SW. CT-NET: A novel convolutional transformer-based network for short-term solar energy forecasting using climatic information. Comput Syst Sci Eng 2023;47(2).

[21] Kumari P, Toshniwal D. Long short term memory–convolutional neural network based deep hybrid approach for solar irradiance forecasting. Appl Energy 2021;295:117061.

[22] Meng M, Song C. Daily photovoltaic power generation forecasting model based on random forest algorithm for north China in winter. Sustainability 2020;12(6):2247.

[23] Aprillia H, Yang H-T, Huang C-M. Short-term photovoltaic power forecasting using a convolutional neural network–salp swarm algorithm. Energies 2020;13(8):1879.

[24] Yu D, Choi W, Kim M, Liu L. Forecasting day-ahead hourly photovoltaic power generation using convolutional self-attention based long short-term memory. Energies 2020;13(15):4017.

[25] Abdulai D, Gyamfi S, Diawuo FA, Acheampong P. Data analytics for prediction of solar PV power generation and system performance: A real case of bui solar generating station, ghana. Sci Afr 2023;21:e01894.

[26] Ahn HK, Park N. Deep RNN-based photovoltaic power short-term forecast using power IoT sensors. Energies 2021;14(2):436.

[27] Harrou F, Kadri F, Sun Y. Forecasting of photovoltaic solar power production using LSTM approach. Adv Stat Model Forecast Fault Detect Renew Energy Syst 2020;3.

[28] Gao M, Li J, Hong F, Long D. Day-ahead power forecasting in a large-scale photovoltaic plant based on weather classification using LSTM. Energy 2019;187:115838.

[29] Mbungu NT, Bansal RC, Naidoo RM, Siti MM, Ismail AA, Elnady A, et al. Performance analysis of different control models for smart demand–supply energy management system. J Energy Storage 2024;90:111809.

[30] Batiyah S, Sharma R, Abdelwahed S, Zohrabi N. An MPC-based power management of standalone DC microgrid with energy storage. Int J Electr Power Energy Syst 2020;120:105949.

[31] Gao Y, Matsunami Y, Miyata S, Akashi Y. Model predictive control of a building renewable energy system based on a long short-term hybrid model. Sustainable Cities Soc 2023;89:104317.

[32] Vrettos E, Gehbauer C. A hybrid approach for short-term PV power forecasting in predictive control applications. In: IEEE milan powerTech. 2019, p. 1–6.

[33] Pataro IM, Gil JD, da Costa MVA, Roca L, Guzmán JL, Berenguel M. A stochastic nonlinear predictive controller for solar collector fields under solar irradiance forecast uncertainties. IEEE Trans Control Syst Technol 2024;32(1):99–111.

[34] Li S, Fairbank M, Johnson C, Wunsch DC, Alonso E, Proao JL. Artificial neural networks for control of a grid-connected rectifier/inverter under disturbance, dynamic and power converter switching conditions. IEEE Trans Neural Netw Learn Syst 2013;25(4):738–50.

[35] Perera M, De Hoog J, Bandara K, Senanayake D, Halgamuge S. Day-ahead regional solar power forecasting with hierarchical temporal convolutional neural networks using historical power generation and weather data. Appl Energy 2024;361:122971.

[36] Michael NE, Bansal RC, Ismail AAA, Elnady A, Hasan S. A cohesive structure of bi-directional long-short-term memory (BiLSTM)-GRU for predicting hourly solar radiation. Renew Energy 2024;222:119943.

[37] Rangelov D, Boerger M, Tcholtchev N, Lämmel P, Hauswirth M. Design and development of a short-term photovoltaic power output forecasting method based on random forest, deep neural network and LSTM using readily available weather features. IEEE Access 2023;11:41578–95.

[38] Khotsirwong N, Boonraksa T, Boonraksa P, Fangsuwannarak T, Boonsrirat A, Marungsri B. Weekly power generation forecasting using deep learning techniques: Case study of a 1.5 MWp floating PV power plant. In: IEEE international conference on power, energy and innovations. ICPEI, 2022, p. 1–4.

[39] Cannizzaro D, Aliberti A, Bottaccioli L, Macii E, Acquaviva A, Patti E. Solar radiation forecasting based on convolutional neural network and ensemble learning. Expert Syst Appl 2021;181:115167.

[40] Heo J, Song K, Han S, Lee D-E. Multi-channel convolutional neural network for integration of meteorological and geographical features in solar power forecasting. Appl Energy 2021;295:117083.

[41] Zang H, Cheng L, Ding T, Cheung KW, Wei Z, Sun G. Day-ahead photovoltaic power forecasting approach based on deep convolutional neural networks and meta learning. Int J Electr Power Energy Syst 2020;118:105790.

[42] Brunton SL, Kutz JN. Data-driven science and engineering: Machine learning, dynamical systems, and control. Cambridge University Press; 2022.

[43] Mbungu NT, et al. A dynamic coordination of microgrids. Appl Energy 2025;377:124486.

[44] Breiman L. Random forests. Mach Learn 2001;45:5–32.

[45] Cheng H, Ding X, Zhou W, Ding R. A hybrid electricity price forecasting model with Bayesian optimization for german energy exchange. Int J Electr Power Energy Syst 2019;110:653–66.

[46] Dhata EF, Kim CK, Kim H-G, Kim B, Oh M. Site-adaptation for correcting satellite-derived solar irradiance: Performance comparison between various regressive and distribution mapping techniques for application in daejeon, South Korea. Energies 2022;15(23):9010.